

Servo Control Design for a High TPI Servo Track Writer With Microactuators

Chin Kwan Thum^{1,2}, Chunling Du¹, Jingliang Zhang¹, Kim Piew Tan¹, Ben M. Chen², *Fellow, IEEE*, and Eng Hong Ong¹

¹A*STAR Data Storage Institute, Singapore 117608

²Department of Electrical and Computer Engineering, National University of Singapore, Singapore 117576

This paper proposes modifications to enhance the original generalized Kalman–Yakubovic–Popov (G-KYP) lemma-based sensitivity function shaping technique that Q -parameterizes the controller and solves for the desired finite impulse response filter $Q(z)$ using linear matrix inequalities (LMI) optimization. By representing $Q(z)$ with an infinite impulse response filter and including an extra LMI that is derived based on the bounded real lemma into the original LMI optimization algorithm, our modifications avoid such problems as unnecessary increase and decrease in sensitivity gain at various frequency ranges, large sensitivity peak, degradation in noise rejection, and insufficient stability robustness against plant uncertainty. In other words, the proposed scheme achieves a better compromise between disturbance and noise rejection performance and stability robustness. The proposed control design was applied to a servo track writing platform. Experimental results show that the control design based on our proposed scheme further reduces the true PES NRRO 3σ from 6 nm to 5.7 nm and improves the closed-loop stability robustness by 5.1%.

Index Terms—Control applications, information storage systems, mechatronics, servo track writing.

I. INTRODUCTION

PRESENTLY, the hard disk drive (HDD) is one of the most popular mass data storage devices due to its large storage capacity, fast transfer rate, and low cost. The servomechanism of servo track writing (STW) platform plays an important role in increasing the storage capacity of a HDD. As the track density, measured by track-per-inch (TPI) increases for higher storage capacity annually, the combined effect of various major track misregistration contributors, namely, airflow-induced disk, suspension, and slider vibrations [1] as well as spindle nonrepeatable runout, become more significant. In order to achieve higher TPI numbers, the servo bandwidth of the STW process has to be improved for better disturbance attenuation.

Consequently, a dual-stage actuation STW platform with multiple bandwidth microactuators [2] has been proposed [3]. It has been shown that the use of the second actuation can effectively compensate the effect of motor-, disk, and suspension-induced vibrations [4], especially in STW process [5]. With the emergence of this novel STW platform, various new feedback control designs [6], [7] have been proposed recently. Among these new control designs, the control design based on the original G-KYP lemma based sensitivity function shaping technique for discrete-time system [7] achieved the best result and effectively improved the track density of the new dual-stage actuation STW platform to 425 kTPI.

In the original G-KYP lemma-based sensitivity function shaping scheme, to ensure the convexity of the LMI optimization [8] for the controller design, the resultant sensitivity function is first parameterized using Q -parameterization [9], [10] and the design parameter, $Q(z)$, is represented by a general finite impulse response (FIR) filter. It is well known that when

using Q -parameterization, the resultant sensitivity transfer function, $S(z)$, is represented by

$$S(z) = T_{11}(z) + T_{12}(z)Q(z)T_{21}(z) \quad (1)$$

for some stable transfer functions $T_{11}(z)$, $T_{12}(z)$, and $T_{21}(z)$. Thus, as we will discuss later in Section IV, choosing $Q(z)$ to be a finite-order FIR filter will hinder bandlimited or narrow-band sensitivity gain shaping. Hence, it may cause unnecessary disturbance attenuation and amplification taking places at various frequency ranges. As the resultant complementary sensitivity function, $T(z)$, is given by

$$T(z) = 1 - S(z) \quad (2)$$

choosing $Q(z)$ to be a finite-order FIR filter may also degrade the gain reduction of complementary sensitivity function at the high frequencies and badly affects the noise rejection performance and the robustness of the closed loop stability against plant variation [10], [14].

This paper proposes $Q(z)$ to be represented by an infinite impulse response (IIR) filter instead to avoid all the abovementioned problems. The proposed enhancement aims to achieve bandlimited and narrowband sensitivity gain shaping with a finite-order $Q(z)$. In order not to destroy the convexity of the LMI optimization, poles of $Q(z)$ are added prior to the LMI optimization. A simple guide is provided to select poles for $Q(z)$. Finally, a new LMI derived based on the well-known bounded real lemma is included into the original LMI optimization algorithm so as to enhance its H_∞ stability robustness against plant variation. Simulation and experimental results will show that the proposed enhancement helps to achieve better compromise between disturbance and noise attenuation as well as closed loop stability robustness against plant uncertainty.

The outline of the paper is as follows. Section II presents a brief description of our newly developed STW platform. In Section III, we will give the readers a short recap of the original G-KYP lemma based sensitivity function shaping technique.

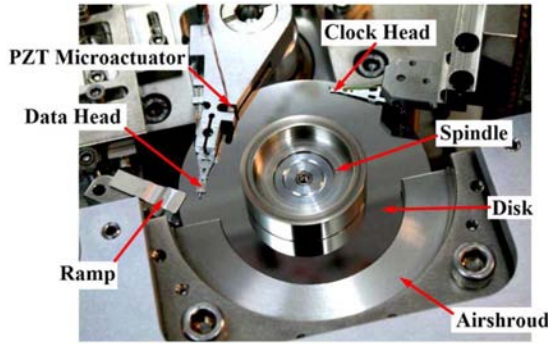


Fig. 1. Zoom-in head-disk-spindle assembly of the STW platform.

TABLE I
PARAMETERS OF THE STW PLATFORM

Spindle	3.5" fluid bearing
Spindle speed	5400 revolutions per minute
Disks	2.5" diameter 1.33 mm thickness Glass material
Numbers of sectors	501

The abovementioned limitations of the original scheme will be highlighted and discussed in further detail, and our proposed enhancement to perfect the original scheme will be described in Section IV. Next, we will apply our proposed enhanced scheme in our STW platform in Section V. Implementation results are presented to see how well our proposed enhanced scheme fares against the original scheme. Finally, we draw some concluding remarks in Section VI.

II. THE STW PLATFORM: A BRIEF SYSTEM DESCRIPTION

Fig. 1 shows the zoom-in view of the head-disk-spindle assembly of our newly developed STW platform, which involves one MicroE as the primary actuator and two PZT microactuators attached to the MicroE-block arms. There are two disk platters that can be accessed by the heads simultaneously. The parameters of the STW platform are listed in Table I.

The MicroE uses its own optical sensing signal as feedback signal and its own servo loop is controlled using a standard proportional-integral-derivative (PID). Here, we focus on the control design for the microactuator with the readback PES as the feedback signal. The control algorithm is implemented with a DSP TMS320C6711.

The frequency response of its microactuator is shown in Fig. 2. Using curve fitting technique, the zeros, poles, and gain of nominal model of the microactuator are given by

$$\begin{aligned} \text{zeros} &= 10^4 \cdot [6.0256 \pm 6.1473j, \\ &\quad -0.2168 \pm 7.2224j, -0.3016 \pm 5.0175j, \\ &\quad -0.1100 \pm 3.1397j, -0.0282 \pm 2.3497] \end{aligned} \quad (3)$$

$$\begin{aligned} \text{poles} &= 10^4 \cdot [-0.3316 \pm 9.4692j, -0.1596 \pm 7.9780j, \\ &\quad -0.1131 \pm 5.6537j, -0.4335 \pm 4.3137j, \\ &\quad -0.1539 \pm 3.0749j, -0.0372 \pm 2.3245j] \end{aligned} \quad (4)$$

$$\text{gain} = 1.8580 \cdot 10^{10}. \quad (5)$$

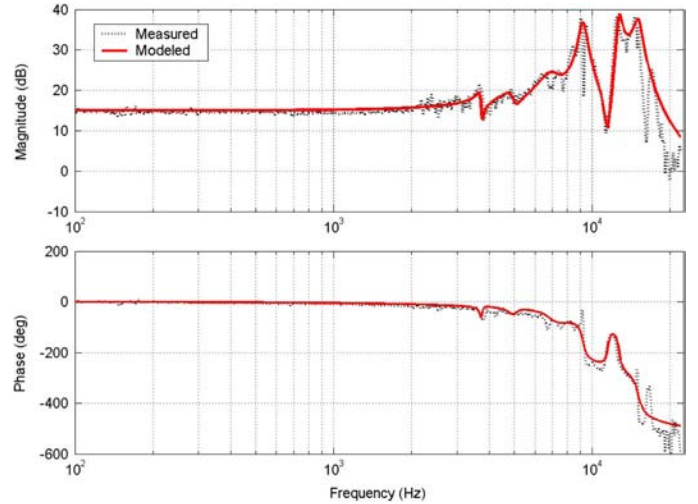


Fig. 2. Frequency response of the microactuator.

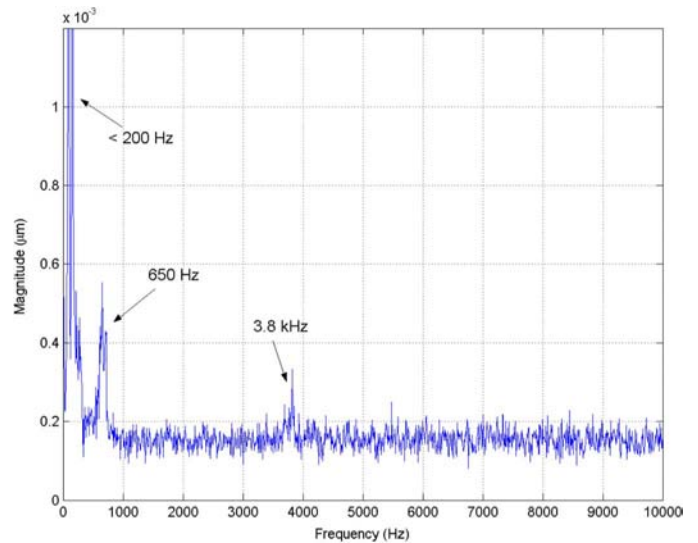


Fig. 3. Measured NRRO power spectrum before servo control.

Its disturbance distribution is reflected in the measured PES NRRO power spectrum in Fig. 3, where the disturbances in the low frequencies (less than 200 Hz) are mostly due to external vibrations and windage, the narrowband NRRO at 650 Hz is due to disk vibration, and the 3.8 kHz are caused by the excited suspension resonance.

Currently, its servo system has been programmed to run at 45 kHz. Due to DSP speed limitation, this platform does not support any controller of order higher than 10. Recently, a 10th-order controller that was designed based on the original scheme was applied to this platform and successfully improved its track density to 425 kTPI [7]. Readers are encouraged to refer to [6] and [7] for a more detailed description of our STW platform.

III. GENERALIZED KYP LEMMA AND ITS ORIGINAL APPLICATION IN SENSITIVITY FUNCTION SHAPING

The G-KYP lemma [11] expresses a necessary and sufficient condition for a given transfer function to satisfy some frequency

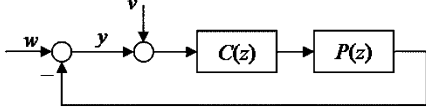


Fig. 4. A simplified block diagram of HDD servo loop with disturbance and noise injected.

domain property, such as bounded magnitude within a specified frequency range, in terms of a linear matrix inequality (LMI). This section discusses how the G-KYP lemma can be used for multiple sensitivity function shaping, i.e., to shape the sensitivity function, $S(z)$, such that the closed loop system is stable and for some prescribed positive scalars, r_i and frequency ranges, $[f_{i1}, f_{i2}]$, $i = 1, \dots, N$

$$|S(f_i)| \leq r_i, \quad f_{i1} \leq f_i \leq f_{i2} \quad (6)$$

and thus able to reject disturbance w in $[f_{i1}, f_{i2}]$ when $r_i < 1$. A simplified block diagram of HDD servo loop is shown in Fig. 4. Note that v represents the measurement noise and the transfer function from w to the controlled output y , $S(z)$, is given by

$$S(z) = \frac{1}{1 + C(z)P(z)} \quad (7)$$

where $P(z)$ is the transfer function of the plant to be controlled and the transfer function of the controller is represented by $C(z)$. In this section, we will also discuss the limitations of the original scheme. We will discuss the details of the proposed enhancement that aims to avoid these limitations in the next section.

For a given transfer function $G(z)$ ($z \in \Lambda$, $\Lambda = \{e^{j\omega}\}$) and a Hermitian matrix

$$\Pi = \begin{bmatrix} \Pi_{11} & \Pi_{12} \\ \Pi_{12}^* & \Pi_{22} \end{bmatrix} \in \mathbf{H}_{m+p}, \Pi_{11} \in \mathbf{H}_p, \Pi_{11} \geq 0 \quad (8)$$

denote

$$\sigma(G, \Pi) = \begin{bmatrix} G \\ I_m \end{bmatrix}^* \Pi \begin{bmatrix} G \\ I_m \end{bmatrix} \quad (9)$$

where $*$ stands for the complex conjugate transpose of a matrix and I_m is the identity matrix of dimensions $m \times m$.

Lemma 1: (G-KYP Lemma) [11] For a transfer function $G(\lambda) := \tilde{C}(\lambda I - \tilde{A})^{-1}\tilde{B} + \tilde{D}$, the condition

$$\sigma(G(\lambda), \Pi) \leq 0, \quad \lambda \in \Lambda \quad (10)$$

holds if and only if there exist Hermitian matrices U and $V \geq 0$ such that

$$\begin{bmatrix} \Gamma(U, V, \tilde{C}, \tilde{D}) & [\tilde{C} \quad \tilde{D}]^* \Pi_{11} \\ \Pi_{11} [\tilde{C} \quad \tilde{D}] & -\Pi_{11} \end{bmatrix} \leq 0 \quad (11)$$

holds, where

$$\begin{aligned} \Gamma(U, V, \tilde{C}, \tilde{D}) := & \begin{bmatrix} \tilde{A} & \tilde{B} \\ I & 0 \end{bmatrix}^* \Sigma \begin{bmatrix} \tilde{A} & \tilde{B} \\ I & 0 \end{bmatrix} \\ & + \begin{bmatrix} 0 & \tilde{C}^* \Pi_{12} \\ \Pi_{12}^* \tilde{C} & \tilde{D}^* \Pi_{12} + \Pi_{12}^* \tilde{D} + \Pi_{22} \end{bmatrix} \end{aligned} \quad (12)$$

and

$$\Sigma = \begin{bmatrix} -U & V \\ V & U - (2 \cos \omega_l) V \end{bmatrix} \quad (13)$$

for low-frequency range $\omega \leq \omega_l$

$$\Sigma = \begin{bmatrix} -U & e^{j\omega_c} V \\ e^{-j\omega_c} V & U - (2 \cos \omega_d) V \end{bmatrix} \quad (14)$$

$$\omega_c = \frac{\omega_1 + \omega_2}{2}, \quad \omega_d = \frac{\omega_2 - \omega_1}{2} \quad (15)$$

for middle-frequency range $\omega_1 \leq \omega \leq \omega_2$, and

$$\Sigma = \begin{bmatrix} -U & -V \\ -V & U + (2 \cos \omega_h) V \end{bmatrix} \quad (16)$$

for high-frequency range $\omega \geq \omega_h$.

For SISO, letting $G(z) = S(z)$ and

$$\begin{aligned} \Pi = \begin{bmatrix} 1 & 0 \\ 0 & -r^2 \end{bmatrix} & \Rightarrow \sigma(G, \Pi) \\ & = |S|^2 - r^2 \leq 0 \end{aligned} \quad (17)$$

then (17) describes the specification (6) on gain of $S(z)$ for a specific frequency range.

Note that when $G(z)$ involves a general form of controller to be designed, (11) generally cannot be convexified since the matrix U is not positive definite and the standard Schur complement cannot be applied. This is why the authors of the original scheme proposed to Q -parameterize $C(z)$ [7]. By choosing the free design parameter $Q(z)$ to be a n th-order FIR filter, i.e., $Q(z) = q_0 + q_1 z^{-1} + q_2 z^{-2} + \dots + q_n z^{-n}$, the resultant $S(z)$ can then be realized by a state space description such that the set of coefficients of $Q(z)$, $q = [q_0 \quad q_1 \quad \dots \quad q_n]$, exists in \tilde{C} and \tilde{D} only. In this case, (11) defines an LMI in terms of variables U, V , and q . Consequently, the design parameter q , can be computed via a convex optimization [8].

IV. AN ENHANCED GENERALIZED KYP LEMMA-BASED SENSITIVITY FUNCTION SHAPING TECHNIQUE

In this paper, we propose to represent $Q(z)$ with a n th-order IIR filter. For analytical purposes, from (1), we express the resultant $S(z)$ as

$$S(z) = T_Q(z)T_{11}(z) \quad (18)$$

with

$$T_Q(z) = 1 - T_{12}(z)Q(z)T_{21}(z)T_{11}^{-1} \quad (19)$$

from which

$$\text{pole}\{T_Q(z)\} \supset \text{pole}\{Q(z)\}. \quad (20)$$

If $T_Q(z)$ is desired to have n specific poles, we will let $Q(z)$ be a n th-order IIR filter whose poles are set to be those n specific poles. Poles of $Q(z)$ will be inserted prior to the LMI optimization. This ensures the convexity of the optimization algorithm. The LMI optimization will search for the existence of the design parameter vector, q , which determines the zero polynomial of $Q(z)$, such that the prescribed specifications of $S(z)$ can be satisfied.

A. Selection of Poles of $Q(z)$ and Simulation Results

Here, we provide three examples as an illustrative guide for the selection of poles for $Q(z)$ to achieve low-frequency disturbance rejection, midfrequency narrowband disturbance re-

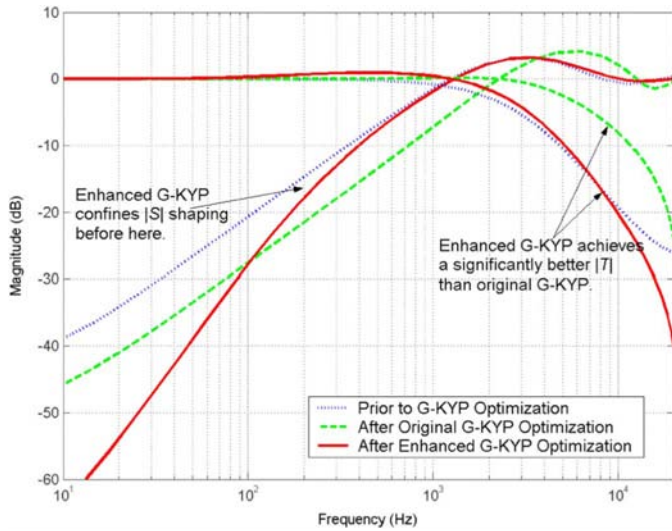


Fig. 5. Case 1: $|S|$ and $|T|$.

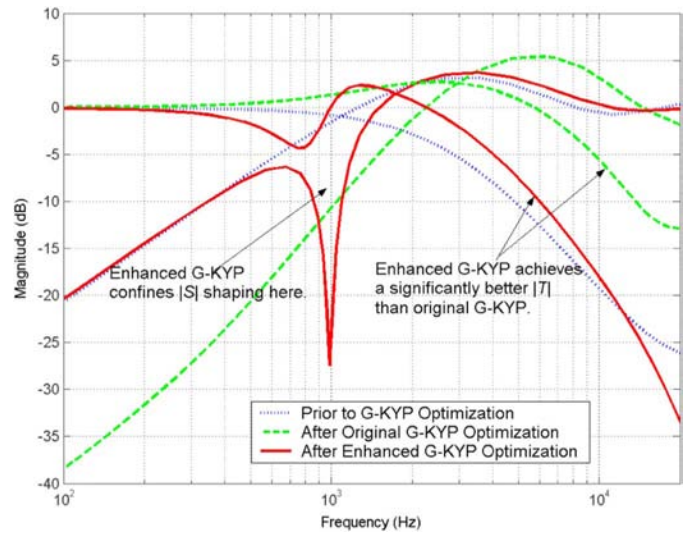


Fig. 7. Case 2: $|S|$ and $|T|$.

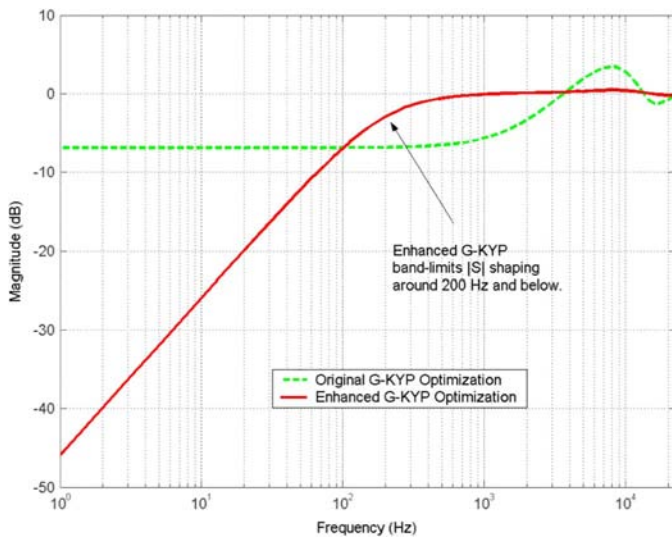


Fig. 6. Case 1: $|T_Q|$.

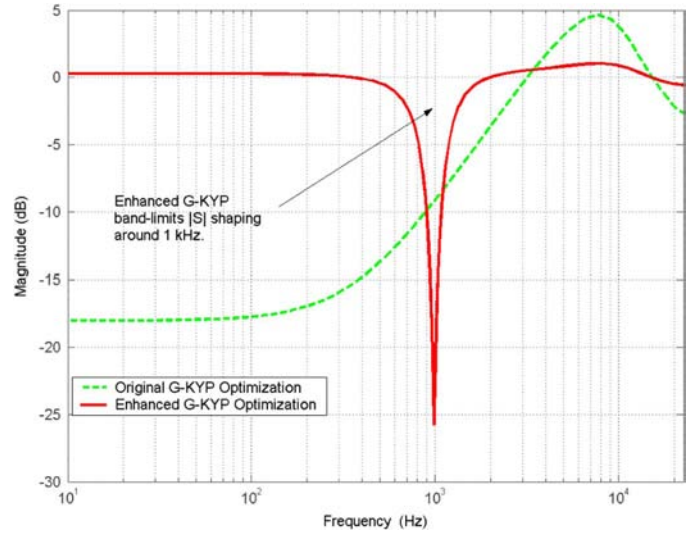


Fig. 8. Case 2: $|T_Q|$.

jection, and high-frequency narrowband disturbance rejection as shown in Figs. 5–10. These discrete poles are derived from their continuous-time counterparts either using the bilinear or matched pole-zero rule. To verify the effectiveness of the enhanced scheme, the servo system is also designed based on the same design specifications using the original scheme for comparisons.

In our examples, the system to be controlled is chosen to be a second-order proper nonminimum phase plant, i.e., $P_1(z)$ is given by

$$P_1(z) = \frac{-0.22494(z - 1.965)(z + 0.999)}{(z - 0.999)(z - 0.03528)}$$

$$\leftrightarrow \begin{bmatrix} A_1 & B_1 \\ C_1 & D_1 \end{bmatrix}.$$

The sampling rate is set to be 45 kHz, which is the same as the sampling rate of our STW platform servo system.

Following the method given in [7], the design parameters F and L for Q -parameterization is chosen based on

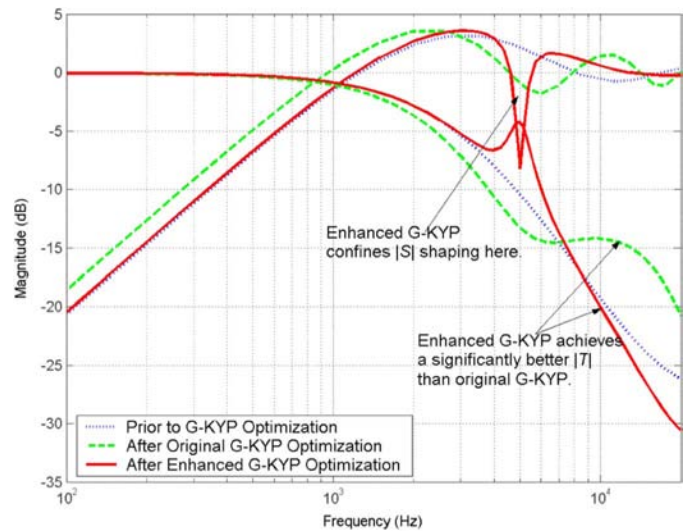
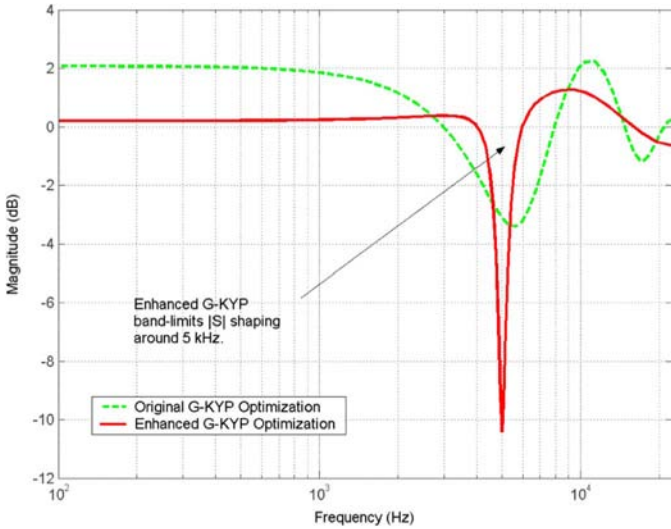


Fig. 9. Case 3: $|S|$ and $|T|$.

a standard LQG design using MATLAB commands $F = dlqr(A_1, B_1, C_1' C_1, R)$ and $L = dlqe(A_1, B_1, C_1, W_d, W_v)$,


 Fig. 10. Case 3: $|T_Q|$.

where R , W_d , and W_v are replaced with identity matrices. Based on the design specifications for each case, a set of LMIs are derived that will be used to compute a suitable q such that the design specifications are met.

1) *Rejecting Low-Frequency Disturbances*: In this case, a first-order IIR $Q(z)$ is used. The desired specifications for $S(z)$ are set as

$$\text{Spec.}(a) : |S| \leq -25 \text{ dB}, \quad f \leq 100 \text{ Hz}$$

$$\text{Spec.}(b) : |S| \leq 0 \text{ dB}, \quad f \leq 1 \text{ kHz}$$

$$\text{Spec.}(c) : |S| \leq 4.5 \text{ dB}, \quad f \leq 10 \text{ kHz.}$$

Spec.(a) ensures additional rejection of low-frequency disturbances. Spec.(b) guarantees a minimal servo bandwidth of 1 kHz. Spec.(c) helps to restrict the size of $|S|$ peak as well as the servo bandwidth. The pole of $Q(z)$ is placed at 200 Hz and discretized using the matched pole-zero rule. After solving the three LMIs corresponding to Spec.(a), (b), (c), $Q(z)$ is computed to be

$$Q(z) = \frac{-0.1161z + 0.06374}{z - 0.9725}. \quad (21)$$

The resultant $|S|$ and $|T|$ are shown in Fig. 5. Fig. 5 also shows the resultant $|S|$ and $|T|$ when the servo system is designed using the original scheme. The FIR $Q(z)$ is given by

$$Q(z) = -0.6034 - 0.4392z^{-1}. \quad (22)$$

Their corresponding $T_Q(z)$ are shown in Fig. 6. As seen in Figs. 5 and 6, as the bandlimited $|S|$ shaping is unable to take place when using the original scheme with the first-order FIR $Q(z)$, unnecessary extra disturbance attenuation took place and is extended all the way beyond 2 kHz despite that Spec.(a) only requires extra attenuation to happen at 100 Hz and below. The resultant servo bandwidth is widened. As a result, the resultant $|S|$ peak is larger and shifted to higher frequencies. The gain reduction of $|T|$ at higher frequencies is badly consequently affected as well. Meanwhile, with the proposed scheme, the band-

limited $|S|$ shaping is possible and takes place at 200 Hz and below. The resultant $|S|$ and $|T|$ at higher frequencies remains the same after optimization as shown in Fig. 5. In this example, when using the original scheme, $T_Q(z)$ does not contain a pole at 200 Hz. Thus, in order to achieve the bandlimited frequency gain shaping similar to the one achieved by the IIR $Q(z)$, the FIR $Q(z)$ would have to be of relatively higher order [15].

2) *Rejecting Midfrequency Narrowband Disturbances*: In this case, second-order IIR $Q(z)$ is used to create a gain notch to achieve midfrequency narrowband disturbance rejection. The desired specifications for $S(z)$ are set as

$$\text{Spec.}(a) : |S| \leq 0 \text{ dB}, \quad f \leq 500 \text{ Hz}$$

$$\text{Spec.}(b) : |S| \leq 0 \text{ dB}, \quad 0.99 \text{ kHz} \leq f \leq 1.1 \text{ kHz}$$

$$\text{Spec.}(c) : |S| \leq 5 \text{ dB}, \quad f \leq 9.8 \text{ kHz}$$

Spec.(a) guarantees a minimal servo bandwidth of 500 Hz. Spec.(b) ensures additional rejection of the mid-frequency disturbance that centers at 1 kHz. Spec.(c) helps to restrict the size of $|S|$ peak as well as the servo bandwidth. The pair of complex poles of $Q(z)$ of damping ratio ζ are placed at 1 kHz and discretized using the bilinear rule. The 3 dB bandwidth of the gain notch can be approximately adjusted by adjusting ζ using the Q -factor rule [16]. And in this case, $\zeta = 0.3$. After solving the three LMIs corresponding to Spec.(a), (b), (c), $Q(z)$ is computed to be

$$Q(z) = \frac{-0.2555z^2 + 0.3722z - 0.1155}{z^2 - 1.902z + 0.9201}. \quad (23)$$

The resultant $|S|$ and $|T|$ are shown in Fig. 7. Fig. 7 also shows the resultant $|S|$ and $|T|$ when the servo system is designed using the original scheme. The FIR $Q(z)$ is given by

$$Q(z) = -1.083 - 0.4222z^{-1} - 0.1613z^{-2} \quad (24)$$

$|T_Q|$ with respective schemes are shown in Fig. 8. As shown in Figs. 7 and 8, with the enhanced scheme, $|T_Q|$ is narrowband around 1 kHz and essentially maintained close to 0 dB at other frequencies. The resultant $|S|$ and $|T|$ at higher frequencies remains the same after optimization as shown in Fig. 7. Hence, unnecessary disturbance and noise attenuation and amplification are avoided. When using the original scheme with the second-order FIR $Q(z)$, the narrowband $|S|$ shaping around 1 kHz is not achievable, and the resultant servo bandwidth is much wider. Consequently, the resultant $|S|$ and $|T|$ at higher frequencies are badly affected. The hump is larger and shifted to higher frequencies. It is noted previously that a higher order FIR $Q(z)$ would be needed to achieve the similar shaping results to the second-order IIR one.

3) *Rejecting High-Frequency Narrowband Disturbances*: In this case, a second-order IIR $Q(z)$ is used to create a gain notch to achieve high-frequency narrowband disturbance rejection. The desired specifications for $S(z)$ are set as

$$\text{Spec.}(a) : |S| \leq 0 \text{ dB}, \quad f \leq 800 \text{ Hz}$$

$$\text{Spec.}(b) : |S| \leq 0 \text{ dB}, \quad 4.98 \text{ kHz} \leq f \leq 5.02 \text{ kHz}$$

$$\text{Spec.}(c) : |S| \leq 5.5 \text{ dB}, \quad f \leq 10 \text{ kHz.}$$

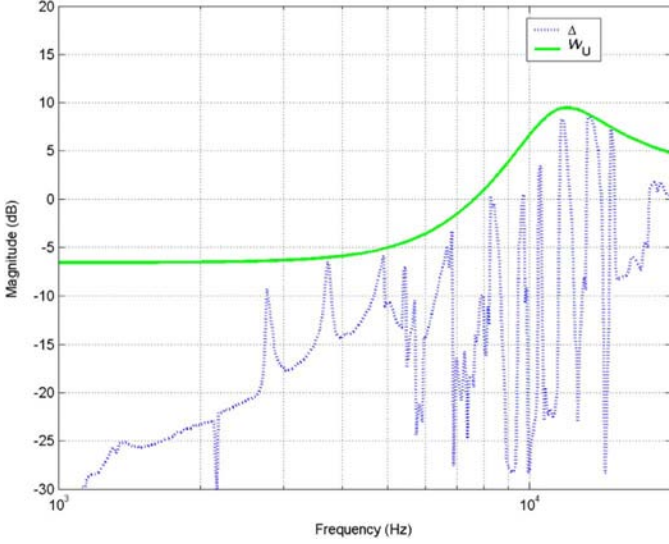


Fig. 11. Multiplicative uncertainty Δ of the microactuator.

Spec.(a) guarantees a minimal servo bandwidth of 800 Hz. Spec.(b) ensures some level of rejection of the high-frequency disturbance that centers at 5 kHz. Spec.(c) helps to restrict the size of $|S|$ peak as well as the servo bandwidth. The pair of complex poles of $Q(z)$ of damping ratio ζ are placed at 5 kHz and discretized using the matched pole-zero rule. Similarly, the 3 dB bandwidth of the gain notch is approximately adjusted using the Q -factor rule. And in this case, $\zeta = 0.1$. After solving the three LMIs corresponding to Spec.(a), (b), (c), $Q(z)$ is computed to be

$$Q(z) = \frac{-0.1874z^2 + 0.3837z - 0.1769}{z^2 - 1.435z + 0.8699}. \quad (25)$$

The resultant $|S|$ and $|T|$ are shown in Fig. 9. Fig. 9 also shows the resultant $|S|$ and $|T|$ when the servo system is designed using the original scheme. The FIR $Q(z)$ is given by

$$Q(z) = -0.1288 + 0.2117z^{-1} + 0.4316z^{-2} \quad (26)$$

$|T_Q|$ with respective schemes are shown in Fig. 10. Similar to Case 2, once again, when using to the original scheme, $|T_Q|$ is not narrowband at 5 kHz, as specified by Spec.(b). The sensitivity function is greatly distorted in order to allow the resultant $S(z)$ to meet all the specifications after the optimization. Unnecessary extra wideband disturbance attenuation happens near 5 kHz. As bounded by the Bode Integral theorem [13], the disturbance attenuation power at the lower frequencies is reduced and another $|S|$ hump happens around 10 kHz. The gain reduction of $T(z)$ at above 10 kHz is badly affected as well. On the other hand, when using the enhanced scheme, $T_Q(z)$ is narrowband at 5 kHz and maintained close to 0 dB at lower frequencies. Thus, the resultant $|S|$ and $|T|$ are essentially unaffected in the frequency range lower than 5 ± 0.02 kHz and the narrowband $|S|$ is achieved.

B. H_∞ Stability Robustness

As seen previously, though representing $Q(z)$ with an IIR filter can help to achieve better bandlimited and narrowband $|S|$

shaping, thus improve the H_∞ stability robustness [10], [14] against plant variation by preventing a serious degradation in the gain reduction of $|T|$ at high frequencies, stability robustness has not really considered during the designing stage.

Assume that the nominal plant has a multiplicative uncertainty, Δ , where $|\Delta| \leq |W_U|$, and $W_U \in RH_\infty$. Then according to the small gain theorem [10], [14], the closed loop system is internally stable for all Δ if and only if $\|T(z)W_U\|_\infty \leq 1$. And based on the bounded real lemma [10], denote that $TW_U(z) := C_U(zI - A_U)^{-1}B_U + D_U$ and

$$\begin{bmatrix} -X_\infty & X_\infty A_U & X_\infty B_U & 0 \\ * & -X_\infty & 0 & C_U' \\ * & * & -\gamma I & D_U' \\ * & * & * & -\gamma I \end{bmatrix} < 0 \quad (27)$$

where X_∞ is a positive symmetric matrix and $\gamma \leq 1$, (27) becomes the sufficient and necessary condition for closed loop stability for all Δ . So we propose to include (27) into the original LMI optimization algorithm for stability robustness consideration when designing $C(z)$. Please note that since

$$\begin{aligned} T(z) &= 1 - S(z) \\ \Rightarrow TW_U(z) &= T_{U1}(z) + T_{U2}(z)Q(z)T_{U3}(z) \end{aligned} \quad (28)$$

where $T_{U1}(z) = (1 - T_{11}(z))W_U(z)$, $T_{U2}(z) = -T_{12}(z)$, and $T_{U3}(z) = T_{21}(z)W_U(z)$, it becomes apparent that q can be made to appear only in C_U and D_U . Thus, the convexity of the LMI optimization algorithm remains intact after the modification.

V. REJECTING LOW-FREQUENCY DISTURBANCES FOR A STW PLATFORM: DESIGN AND IMPLEMENTATION RESULTS

The nominal plant model of the microactuator after notch filters compensation [7] is represented with a *padè* delay model

$$P_0(s) = -5.6324 \frac{s - 2 \cdot \pi \cdot 17000}{s + 2 \cdot \pi \cdot 17000} \quad (29)$$

which needs to be further compensated with an integrator [7] prior to Q -parameterization.

Judging from Fig. 3, it is clear that the servo system contains significantly more noise than disturbance at frequencies above 1 kHz. Since most of the NRRO centers around the low-frequency region, typically around 650 Hz and below 200 Hz, it would be wise if the set of design specifications for $S(z)$ aims to reduce $|S|$ only at the low-frequency range while keeping the servo bandwidth minimal for better noise rejection. Consequently, the desired specifications for $S(z)$ are set as

$$\begin{aligned} \text{Spec.(a)} : |S| &\leq -33 \text{ dB}, \quad f \leq 100 \text{ Hz} \\ \text{Spec.(b)} : |S| &\leq 0 \text{ dB}, \quad f \leq 600 \text{ Hz} \\ \text{Spec.(c)} : |S| &\leq -8.3 \text{ dB}, \quad 625 \text{ Hz} \leq f \leq 675 \text{ Hz} \\ \text{Spec.(d)} : |S| &\leq 9 \text{ dB}, \quad f \geq 11710 \text{ Hz}. \end{aligned}$$

Spec.(a) guarantees serious rejection of low-frequency disturbances. Spec.(b) ensures a minimal servo bandwidth of 600 Hz. Spec.(c) means to reject the narrowband NRRO centering at

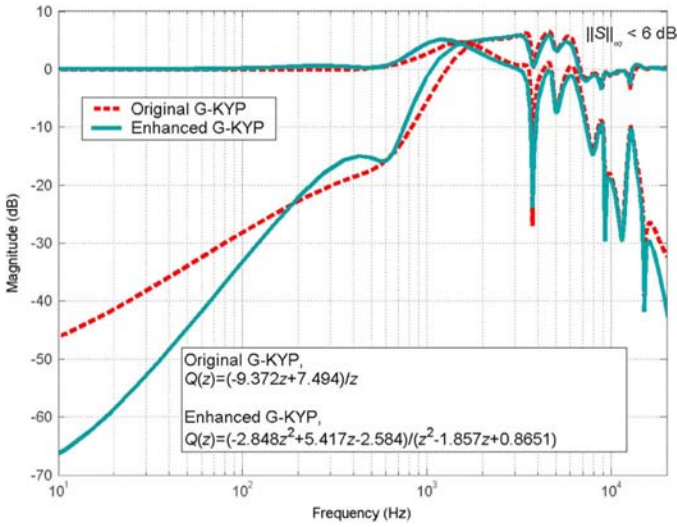


Fig. 12. $|S|$ and $|T|$. Proposed scheme further reduces $|S|$ at frequencies < 200 Hz and maintains an equivalent low gain at around 650 Hz and 3.8 kHz while $|T|$ at frequencies > 1.5 kHz (especially after 15 kHz) improves instead of getting worse.

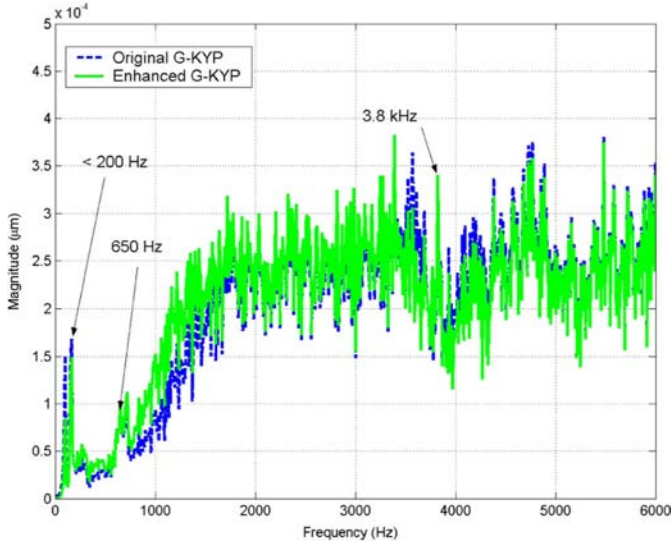


Fig. 13. Measured NRRO power spectrum with servo control. Sudden appearance of peaks at higher frequency is due to the humps in the $|S|$ from 1.2 to 7 kHz with the respectively servo controllers.

650 Hz by 8.3 dB, at least. Finally, Spec.(d) helps to limit the size of $|S|$ peak as well as the servo bandwidth.

To capture the unmodeled dynamics, dozens of frequency response measurements have been carried out. The multiplicative uncertainty, Δ , of microactuator, defined by

$$\Delta(\omega) = \max_i^N \left| \frac{P_i(j\omega) - P_0(j\omega)}{P_0(j\omega)} \right| \quad (30)$$

where N is the number of measurements taken and $P_i(j\omega)$ is the actual frequency response of the precompensated plant at the i th measurement and $P_0(j\omega)$ is the selected frequency response of nominal plant model in (29). As shown in Fig. 11, an approximate bounding function $W_U(s)$ is obtained and given by

$$W_U(s) = 1.26 \frac{s^2 + 5.341 \cdot 10^4 s + 1.934 \cdot 10^9}{s^2 + 3.035 \cdot 10^4 s + 5.221 \cdot 10^9} \quad (31)$$

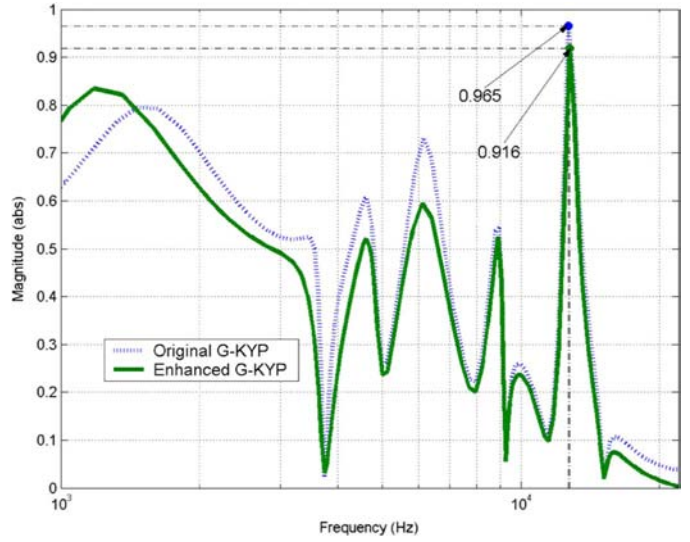


Fig. 14. $|TW_U|$.

In our control design, $W_U(s)$ is discretized using the matched pole-zero rule.

So for H_∞ stability robustness, we include another design specification:

$$\text{Spec.}(e) : \text{minimize } \gamma, \quad \|TW_U\|_\infty < \gamma.$$

Based on Spec.(a) and (c), we decide to use a second-order IIR filter to present $Q(z)$. Poles of $Q(z)$ are decided to be a pair of 650 Hz complex pole of $\zeta = 0.8$, a 3 dB notch wide enough such that Spec.(c) is theoretically feasible and to remove effects of additional zeros at frequencies after 650 Hz. The pair of complex poles are discretized using the bilinear rule. Having solved the LMIs, $Q(z)$ is computed to be

$$Q(z) = \frac{-2.848z^2 + 5.417z - 2.584}{z^2 - 1.857z + 0.8651}. \quad (32)$$

With precompensators, the designed $C(z)$ is found to be a 11th-order controller initially, which is eventually reduced to a 10th-order controller using MATLAB's *balmr* command.

The $|S|$ and $|T|$ of the resultant closed loop system are shown in Fig. 12 in comparison with the resultant $|S|$ and $|T|$ obtained when $C(z)$ is designed with the original scheme. Consistently with the sensitivity gain functions in Fig. 12, the measured PES NRRO power spectrum comparison is shown in Fig. 13. In Fig. 13, as compared to those of the original scheme, we can see that the proposed scheme has further improved NRRO greatly at frequency range below 200 Hz, while maintaining an equally good NRRO rejection performance at around 650 Hz. And at 3.8 kHz, the NRRO caused by the excited suspension resonances has also been reasonably reduced using the proposed scheme. With the proposed scheme, the true PES NRRO 3σ is further improved from 6 to 5.7 nm (5% reduction). $\|TW_U\|_\infty$ is found to be improved from 0.965 to 0.916 (5.1% reduction) as shown in Fig. 14.

VI. CONCLUSION

This paper proposes modifications to enhance the original G-KYP lemma-based sensitivity function shaping technique. Changing $Q(z)$ to an IIR filter allows control designers to perform bandlimited servo loop shaping, thus avoid unnecessary worsening of sensitivity and complementary sensitivity function at higher frequencies. And the inclusion of an H_∞ LMI helps to provide sufficient stability robustness consideration during designing stage. The implementation results on low-frequency disturbance rejection of the STW platform have verified the effectiveness of the proposed scheme. The proposed scheme has achieved 5% more reduction in true PES NRRO 3σ and 5.1% more reduction in $\|TW_U\|_\infty$ over the original scheme.

REFERENCES

- [1] S. Kirpekar and D. B. Bogy, "A study on the efficacy of flow mitigation devices in hard disk drives," *IEEE Trans. Magn.*, vol. 42, no. 6, pp. 1716–1729, Jun. 2006.
- [2] K. Chan and W. Liao, "Shock resistance of a disk-drive assembly using piezoelectric actuators with passive damping," *IEEE Trans. Magn.*, vol. 44, no. 4, pp. 525–532, Apr. 2008.
- [3] L. S. Fan, H. H. Ottesen, T. C. Reiley, and R. W. Wood, "Magnetic recording head positioning at very high track density using a microactuator-based two stage servo system," *IEEE Trans. Ind. Electron.*, vol. 42, no. 3, pp. 222–233, Jun. 1995.
- [4] X. Huang and R. Horowitz, "Robust controller design of a dual-stage disk drive servo system with an instrumented suspension," *IEEE Trans. Magn.*, vol. 41, no. 8, pp. 2406–2413, Aug. 2005.
- [5] G. Guo and J. Zhang, "Control strategies for writing servo tracks narrower than 5 micro inches," presented at the JSME-IIP/ASME-ISPS Joint Conf. Mechatronics for Information and Precision Equipment, Yokohama, Japan, Jun. 16–18, 2003.
- [6] J. Zheng, C. Du, G. Guo, Y. Wang, J. Zhang, Q. Li, and B. Hredzak, "Phase lead peak filter method to high TPI servo track writer with microactuators," in *Proc. Amer. Cont. Conf.*, 2006, pp. 1309–1314.
- [7] C. Du, L. Xie, G. Guo, J. Zhang, Q. Li, B. Hredzak, and J. N. Teoh, "A generalized KYP lemma based control design and application for 425 kTPI servo track writing," in *Proc. Amer. Control Conf.*, 2006, pp. 1303–1308.
- [8] P. Gahinet, A. Nemirovski, A. J. Laub, and M. Chilali, *LMI Control Toolbox*. Natick, MA: MathWorks, 1995.
- [9] S. Boyd and C. H. Barratt, *Linear Controller Design: Limits of Performance*. Englewood Cliffs, NJ: Prentice-Hall, 1981.
- [10] K. Zhou, J. C. Doyle, and K. Glover, *Robust and Optimal Control*. Englewood Cliffs, NJ: Prentice-Hall, 1996.
- [11] T. Iwasaki, G. Meinsma, and M. Fu, "Generalized S-procedure and finite frequency KYP lemma," *Math. Probl. Eng.*, vol. 6, pp. 3587–3592, Nov. 2003.
- [12] G. F. Franklin, J. D. Powell, and M. L. Workman, *Digital Control of Dynamic Systems*, 3rd ed. Englewood Cliffs, NJ: Prentice-Hall, 1998.
- [13] H. W. Bode, *Network Analysis and Feedback Amplifier Design*. New York: Van Nostrand, 1945.
- [14] J. C. Doyle, B. A. Francis, and A. R. Tannenbaum, *Feedback Control Theory*. New York: Macmillian, 1992.
- [15] A. V. Oppenheim, R. W. Schaffer, and J. R. Buck, *Discrete Signal Processing*, 2nd ed. Englewood Cliffs, NJ: Prentice-Hall, 1999.
- [16] A. Antoniou, *Digital Filters: Analysis, Design, and Applications*, 2nd ed. New York: McGraw-Hill, 1993.

Manuscript received January 29, 2007; revised April 24, 2008. Published August 20, 2008 (projected). Corresponding author: C. Thum (e-mail: THUM_Chin_Kwan@dsi.a-star.edu.sg).